frontiers | Frontiers in Materials

TYPE Original Research
PUBLISHED 23 September 2024
DOI 10.3389/fmats.2024.1479398

OPEN ACCESS

EDITED BY
Muhammad Danang Birowosuto,
Łukasiewicz Research Network–PORT Polish Center for Technology Development, Poland

REVIEWED BY
Mohammad Alibakhshikenari,
Universidad Carlos III de Madrid, Spain
Halimjon Khujamatov,
Tashkent University of Information Technology, Uzbekistan
Mazin Mohammed,
University of Anbar, Iraq

*CORRESPONDENCE
Deema Mohammed Alsekait,
dmalsikait@pnu.edu.sa
Pi-Chung Wang,
pcwang@nhu.edu.tw
Ibrahim A. Hameed,
ibib@ntnu.no

RECEIVED 12 August 2024
ACCEPTED 10 September 2024
PUBLISHED 23 September 2024

CITATION
Zhang J, Dong S, Alsekait DM, Khan I, Wang P-C and Hameed IA (2024) Design and performance optimization of a novel lens antenna for emerging beyond 5G wireless applications.
Front. Mater. 11:1479398.
doi: 10.3389/fmats.2024.1479398

Design and performance optimization of a novel lens antenna for emerging beyond 5G wireless applications

Jinhua Zhang[1], Shi Dong[1], Deema Mohammed Alsekait[2]*, Imran Khan[3,4], Pi-Chung Wang[5]* and Ibrahim A. Hameed[6]*

[1]School of Computer Science and Technology, Zhoukou Normal University, Zhoukou, China, [2]Applied College, Department of Computer Science and Information Technology, Princess Nourah Bint Abdulrahman University, Riyadh, Saudi Arabia, [3]Department of Electrical Engineering, University of Engineering and Technology, Lahore, Pakistan, [4]Islamic University Centre for Scientific Research, The Islamic University, Najaf, Iraq, [5]Department of Computer Science and Engineering, National Chung Hsing University, Taichung, Taiwan, [6]Faculty of Information Technology and Electrical Engineering, Norwegian University of Science and Technology, Trondheim, Norway

Introduction: This paper proposes a novel all-dielectric design of lens antenna and its performance is optimized using genetic algorithm (GA). The optimization objective are 1-dB and steady gain that are directly optimized. The GA also optimizes the topological design of the lens.

Methods: The method consists of two main components: the design of the objective function and the initial population selection. The first lens structure fed into the algorithm and the initial population match. The lens has a diameter of 150 mm and a thickness of 30 mm at its thickest point with working frequency of 6–18 GHz. The 3D printing technology is used for the antenna fabrication that reduces the implantation cost.

Results: The experimental results show that the gain and peak aperture efficiency of the proposed antenna are 23.8 dBi and 51.9%, respectively, better than those of the existing designs.

Discussion: It advantages are low-cost, easy to fabricate, simple design, high gain, narrow beams, low side lobes. It can be used in future ultra-wideband (UWB) applications.

KEYWORDS

lens antenna, dielectric material, genetic algorithm, beamforming, 3D printing, miniaturization, 5G antenna, UWB antenna

1 Introduction

In recent years, with the rapid development of modern wireless communication systems, the demand for high-gain, ultra-wideband antennas have been increasing (Kumar et al., 2022). Commonly used high-gain antennas include array antennas (Ullah et al., 2019), transmission array antennas (Liu et al., 2018), parabolic antennas, reflectarray antennas (Ge et al., 2018) and lens antennas (Hao et al., 2019; Fan et al., 2018; Soliman et al., 2022; Farooq et al., 2021; Kumar et al., 2021; Yang et al., 2020; Beguad et al., 2018). Antenna devices are very important for any wireless communication systems. There are various methods to enhance the performance parameters of the antennas such as metamaterials

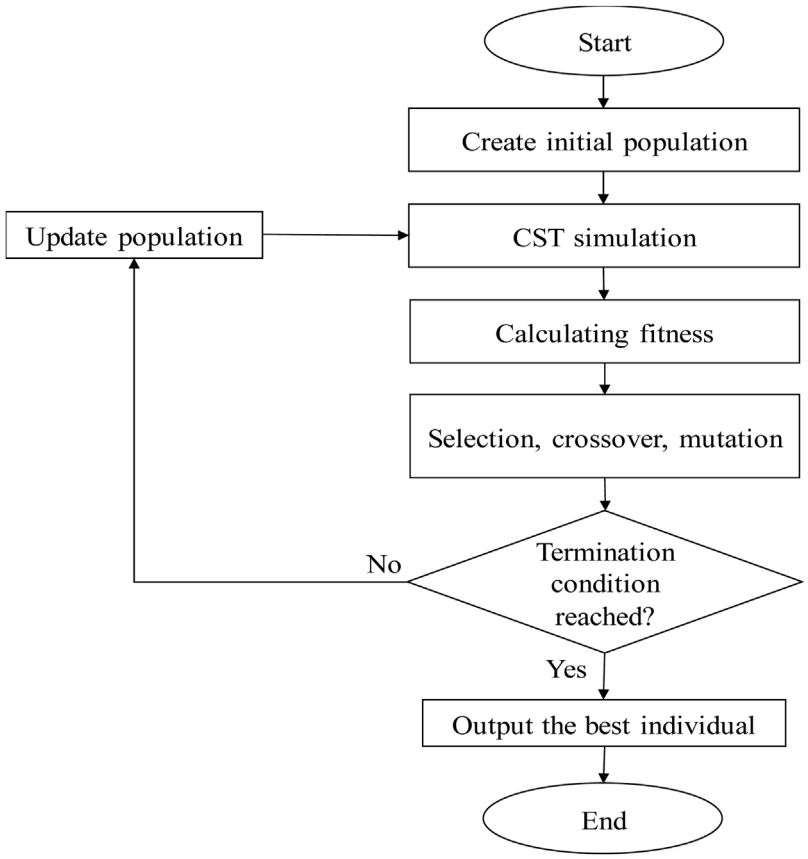

FIGURE 1
Proposed algorithm flowchart.

(Alibakhshikenari et al., 2019; Alibakhshikenari et al., 2016a; Alibakhshikenari et al., 2016b; Alibakhshikenari et al., 2021) and metasurfaces (Alibakhshikenari et al., 2016c; Sadeghzadeh et al., 2016; Alibakhshikenari et al., 2020).

Array antennas mainly increase antenna gain by a large number of array elements and reduce side lobes by adjusting the excitation amplitude and phase. They require a complex feeding network and high production costs (Karami et al., 2022). Transmission array antennas have the advantages of high gain, low profile, and easy processing, but they require specific design of the units and use the units to form an array. The design and formation of the units are usually complicated. Reflection array/surface antennas have the problem of feed source shielding (Srivastava et al., 2020; Li et al., 2023). Lens antennas have the advantages of low side lobes, narrow beams, high gain, and simple manufacturing, but the materials used have dispersion effects, and the lens needs to be designed according to a fixed frequency point for phase design, which limits the bandwidth of the lens antenna. In order to solve this problem, researchers at home and abroad have made great efforts in recent years (Ikram et al., 2024; Liu et al., 2021; Lee and Yoon, 2017).

Lens antennas usually include convex lens antennas (Cicchetti et al., 2020; Lee et al., 2021), Luneburg lens antennas (Feng et al., 2019), Fresnel lens antennas (Jeong and Ghalichechian, 2020; Wang et al., 2024a), gradient refractive index lens antennas (Jeong and Ghalichechian, 2020), etc. Due to their large size, convex lenses and Luneburg lenses are limited in their application in many wireless communication systems. Reference (Jeong and Ghalichechian, 2020) proposed a Fresnel lens antenna with a 3-dB gain bandwidth of 6.7%, aperture efficiency of only 10%, and maximum measured gain of 22.46 dBi. Reference (Wang et al., 2024a) proposed a method to improve the aperture efficiency of lens antennas by performing phase smoothing compensation on the spherical waves reaching the lens surface to achieve high gain and high aperture efficiency of the lens antenna. The measured maximum gain was 38.9 dBi, the maximum aperture efficiency was 59%, and the 2-dB gain bandwidth was 32.5%. Reference (Poyanco et al., 2022) proposed a gradient refractive index lens antenna, which achieved the change of the equivalent dielectric constant by changing the filling ratio of the material, and processed the lens using 3D printing technology. The measured results show that The maximum measured gain is 24 dBi, and the maximum aperture efficiency is 41%. Although the above research has achieved good results, the antenna indicators are not comprehensively considered in the process of designing the lens antenna, and multiple performance indicators cannot be taken into account.

In order to solve the above problems, this paper proposes an all-dielectric lens antenna fed by a ridge horn antenna. Aiming at the requirements of wide bandwidth, high gain and wide 1-dB gain bandwidth, it is optimized by multi-objective genetic algorithm.

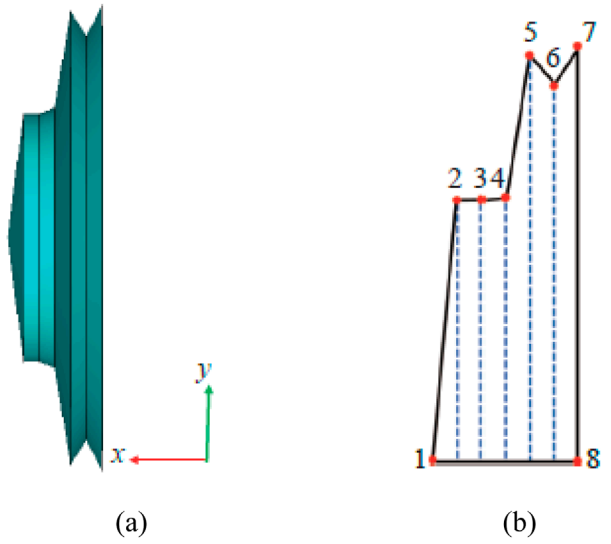

FIGURE 2
Lens design. **(A)** Structure; **(B)** corresponding curve.

TABLE 1 Parameters configuration for optimization.

Parameter	Value
Number of variables	5
Population size	10
Optimized Frequency	6–8 GHz
Target 1-dB gain bandwidth B (%)	100
Termination condition	F(best) remains unchanged after 15 iterations
Target gain $G_i(x)$	(18, 19, 20, 21, 21, 22, 23, 23, 24, 24, 24, 25, 25)

TABLE 2 Design parameters of the proposed antenna.

Parameter	Value (mm)
y_1	0
y_2	46.6
y_3	49.1
y_4	54.8
y_5	64.1
y_6	67.4
y_7	75.0
y_8	0

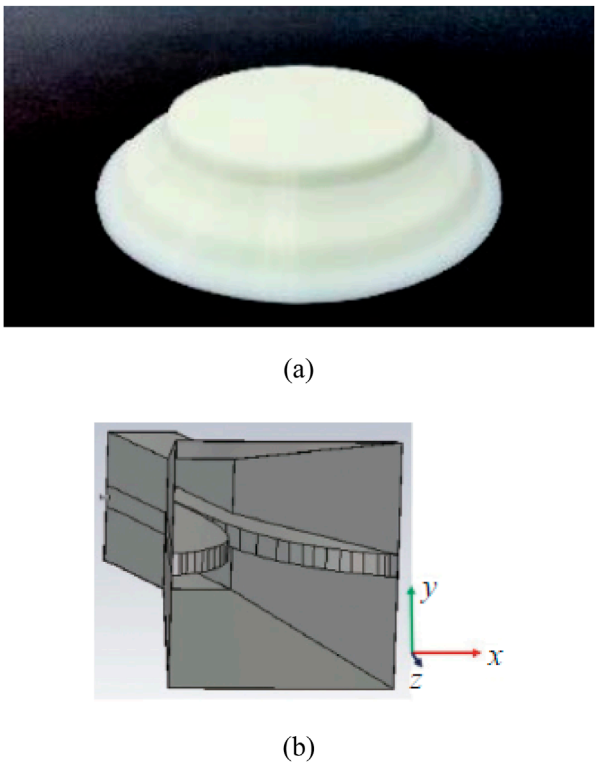

FIGURE 3
Prototype of the proposed antenna structure. **(A)** Lens; **(B)** Horn antenna.

The lens is processed by 3D printing technology and measured in a microwave darkroom. The results show that the gain of the feed antenna is increased by 6.4–10 dBi after loading the lens in the range of 6–18 GHz, and the maximum gain is 23.8 dBi at 17 GHz. The 1-dB gain bandwidth is 12–18 GHz (relative bandwidth 40%), and the maximum aperture efficiency reaches 51.9%, which can meet the application requirements of broadband high-gain wireless systems.

The remainder of this paper is organized as follows. In Section 2, the proposed design is discussed in terms of graphical diagrams and mathematical formulations. In Section 3, the experimental results and analysis is performed. In Section 4, the conclusions are described.

2 Antenna design

2.1 Structural design and algorithm optimization

In order to shorten the design cycle and improve the design efficiency, this paper adopts genetic algorithm to assist the design of lens antenna. To automate the search for the optimized antenna shape in an efficient way, genetic algorithm is a good candidate of optimization methods in the simulation-based. The algorithm flow is shown in Figure 1. There are two key parts in the algorithm, one is the selection of initial population, and the other is the design of objective function. The initial population corresponds to the initial

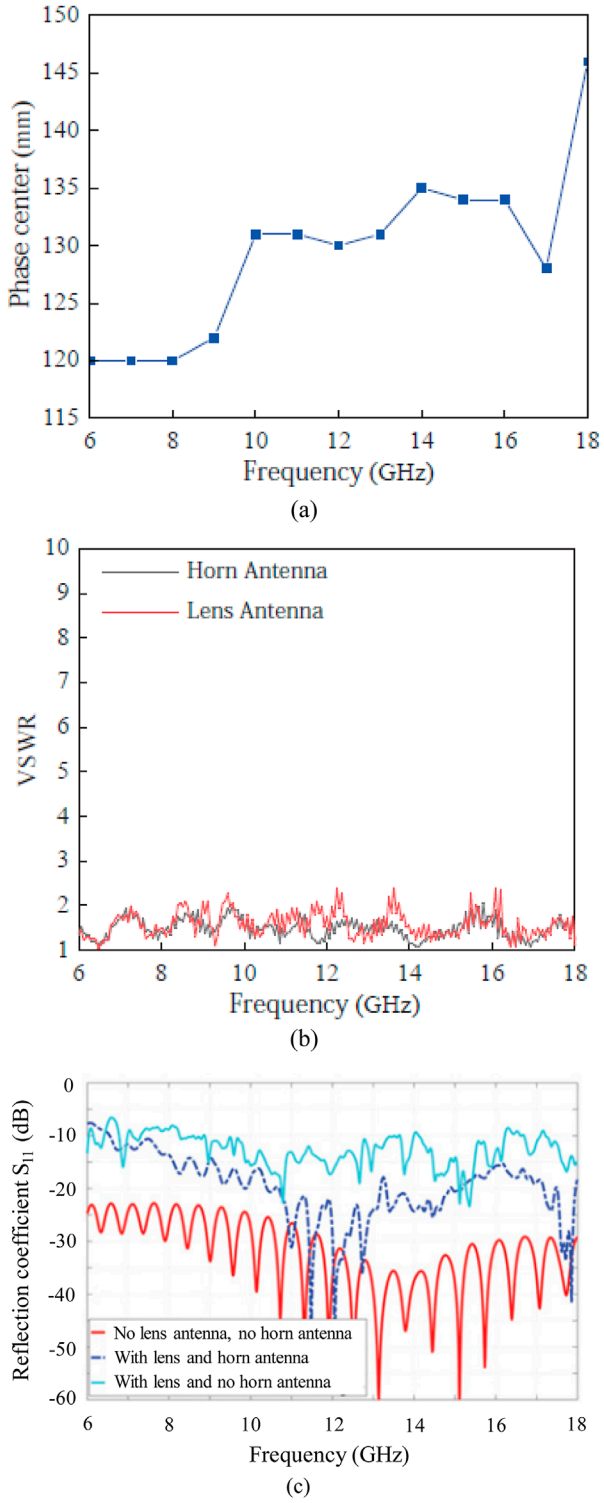

FIGURE 4
Performance evaluation of phase center change and VSWR of the proposed antenna. **(A)** Phase center change; **(B)** VSWR (measured); **(C)** S_{11}.

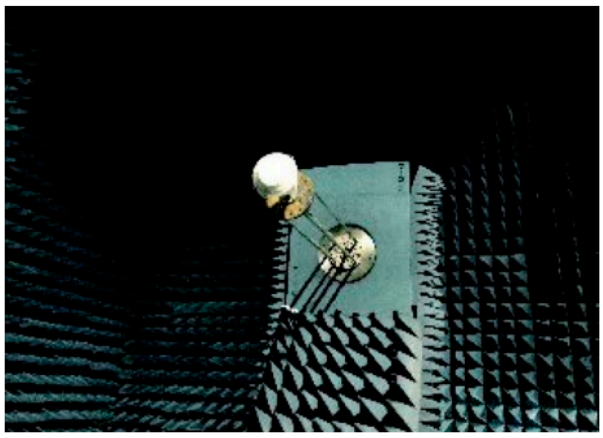

FIGURE 5
Actual measurement setup.

lens structure imported into the algorithm. If the initial structure of the lens is not designed reasonably, the optimization time will be too long and the objective function will not converge (Rahman et al., 2024). The objective function corresponds to the expected effect of the lens antenna. If the objective function is set too harshly, it will lead to the objective function not converging (Dai et al., 2024; Dai et al., 2022; Sun et al., 2022).

In order to improve the degree of freedom of design and reduce the optimization time, a rotating body similar to a convex lens is selected as the initial optimization structure. The focal diameter ratio of the lens is about 1. The initial structure is fixed at 117 mm away from the feed horn surface (Sun et al., 2021; Wen et al., 2022; Li et al., 2024). The initial structure is formed by rotating an irregular plane surrounded by a closed curve around the x-axis, as shown in Figure 2A. The initial structure is a dielectric rotating body with a diameter of 150 mm and a height of 30 mm (Figure 2B). For ease of processing, the material of the lens is set to 3D printing material polylactic acid (PLA) during the simulation process. The dielectric constant of PLA is 2.72 (Khan et al., 2024) within 6–18 GHz, and the loss tangent is 0.008 (Xiao et al., 2023; Wang et al., 2022; Xiao et al., 2017). The corresponding curve is determined by 8 points with different positions, among which points 1, 7 and 8 are fixed and used to determine the thickness and aperture of the lens, while ensuring that the bottom surface of the lens is a flat structure to facilitate fixation with the feed antenna. The positions of the remaining five points are used as optimization variables to optimize the lens structure.

During the optimization process, an initial population is first created. The initial population is an $n \times N$ matrix, where n represents the number of optimization parameters and N represents the size of the initial population (Wang et al., 2024b; Wang et al., 2024c; Li et al., 2021). The optimization parameters in this paper are the coordinate values of points 2 to 6 $[y_2, y_3, y_4, y_5, y_6]$. Considering the optimization effect and optimization time, N is set to 10. The algorithm calls CST to model and simulate the initial structure, and the simulation results are used to calculate the objective function $F(x)$. In each iteration, the fitness value of each individual in the population is calculated, and the individuals are screened using the roulette method. Individuals with high fitness (small $F(x)$) will be retained, and then crossover and mutation will be performed. In order to prevent the loss of the optimal solution and accelerate the convergence of the algorithm, the elite strategy is introduced with

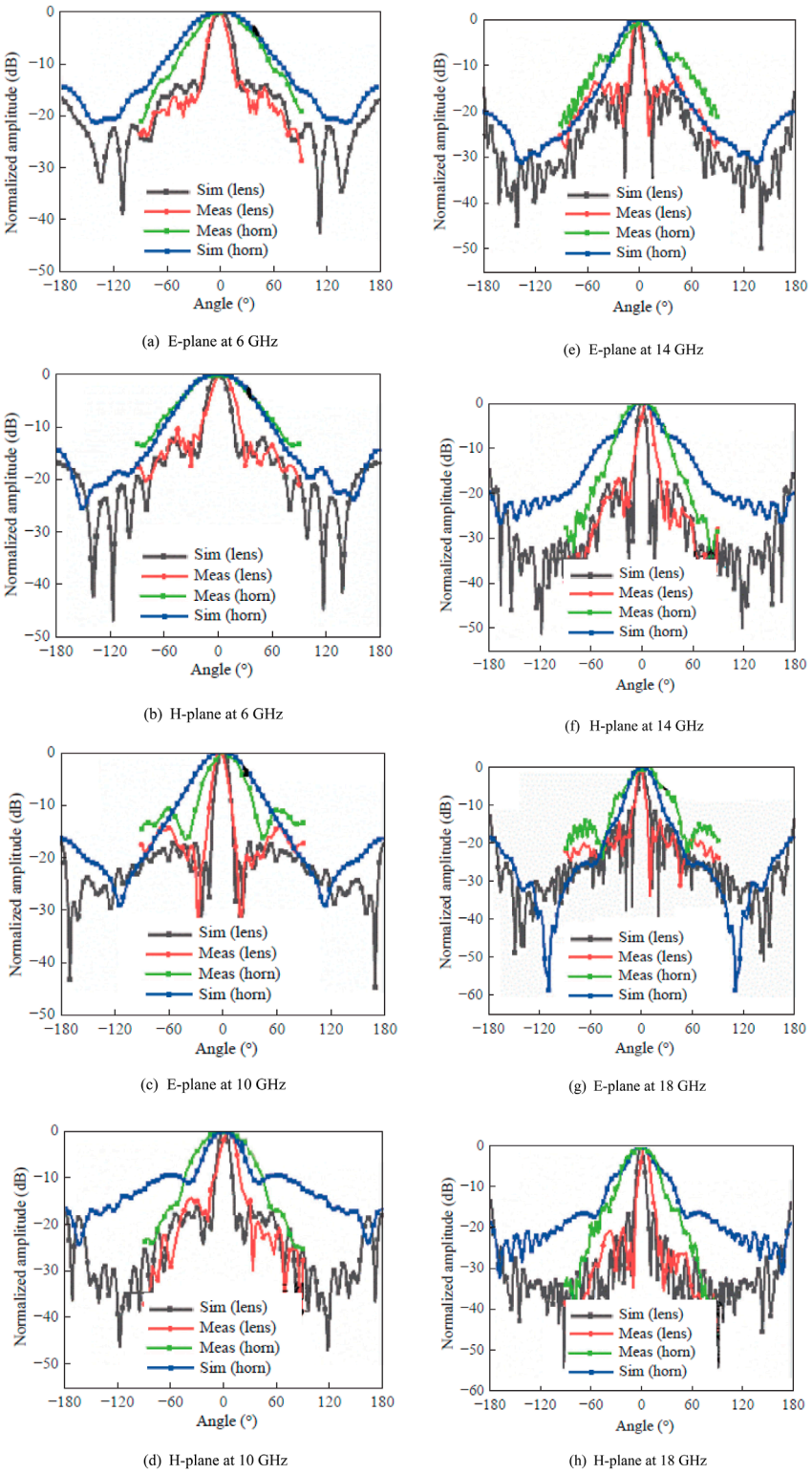

FIGURE 6
Comparison of simulated and measured radiation patterns of the antenna at different frequencies. **(A)** E-plane at 6 GHz **(B)** H-plane at 6 GHz **(C)** E-plane at 10 GHz **(D)** H-plane at 10 GHz **(E)** E-plane at 14 GHz **(F)** H-plane at 14 GHz **(G)** E-plane at 18 GHz **(H)** H-plane at 18 GHz.

reference to the non-dominated sorting genetic algorithm (NSGA-II) (Hao et al., 2022; Liu et al., 2023; Wang et al., 2023), which retains the excellent individuals in the parent generation and directly passes them to the offspring. After crossover and mutation, the best individual of the parent generation replaces the worst individual in the new population. In order to keep the population size unchanged,

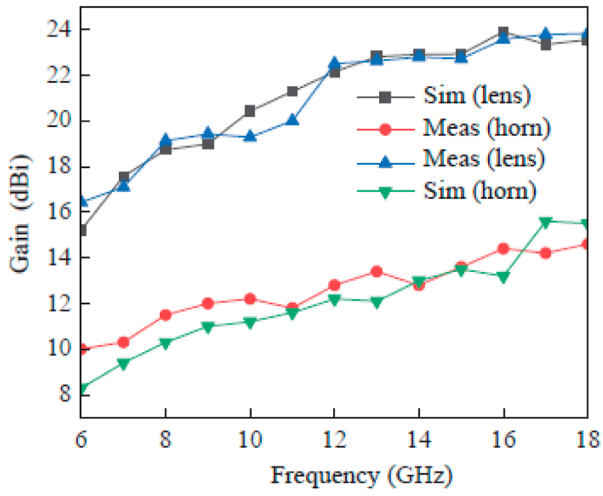

FIGURE 7
Comparison of simulated and measured gain of the antenna.

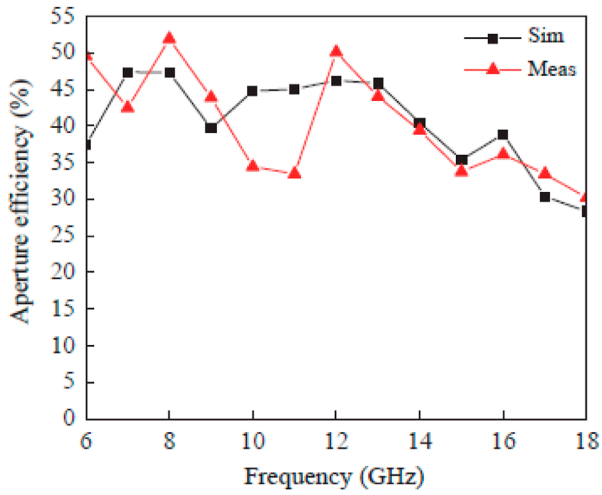

FIGURE 8
Comparison of simulated and measured aperture efficiency.

the algorithm will generate new individuals by random generation when eliminating unqualified individuals (Zhang et al., 2023). The objective function value F(best) corresponding to the best individual in each generation of the population will be recorded. If F(best) still does not change after 15 iterations, the iteration ends and the lens structure corresponding to the best individual is derived. Otherwise, the iteration continues.

2.2 Objective function

The objective function $F(x)$ is expressed as in Equation 1:

$$F(x) = \omega_1 f_1(x) + \omega_2 f_2(x)$$
$$x = [x_1, x_2, \ldots, x_N] \quad (1)$$

Where, ω_1 and ω_2 are the weights of the two optimization objectives respectively; x represents the optimization population, and when $x = x_N$, it indicates that the objective function of the N th individual (lens) in the population is currently being calculated, and the size of N is equal to the number of individuals in the population (Yang et al., 2023a; Chen et al., 2024; Zha et al., 2024); The gain optimization $f_1(x) = \sum_{i=\min f}^{\max f} Q_i(x)$, min f and max f are 6GHz and 18 GHz respectively, $Q_i(x) = \begin{cases} G_i(x) - R_i(x), G_i(x) \geq R_i(x) \\ 0, \text{else} \end{cases}$, $G_i(x)$ and $R_i(x)$ represents the target gain and actual gain respectively. When the actual gain is greater than the expected value, $Q_i(x) = 0$, otherwise $Q_i(x)$ is equal to the difference between the target gain and the actual gain (Wang et al., 2024d).

Bandwidth optimization $f_2(x) = B - \text{Band}(x)/K$, K is a real number greater than 1, by adjusting the size of $f_2(x)$ to make $f_1(x)$ and $f_2(x)$ at the same level, in this paper K is set to 5, B represents the target 1-dB gain bandwidth, Band(x) represents the current individual 1-dB gain bandwidth (Wen et al., 2024a; Wen et al., 2024b), $\text{Band} = f_{\max} - f_{\min}/(f_{\max} + f_{\min}/2) \times 100\%$, $f_{\max}$ and $f_{\min}$ are the maximum frequency and minimum frequencies corresponding to the maximum gain drop of 1-dB.

During the optimization process, each individual x will correspond to an $F(x)$. When $F(x)$ approaches 0, the individual approaches the ideal individual. During the iteration process, the individual with smaller $F(x)$ has a greater probability of being selected (Zhou et al., 2024a; Yang et al., 2023b). The individual will pass on its genes to the next-generation through crossover and mutation. Therefore, as the iteration proceeds, the individuals in the population will become closer to the ideal situation. After reaching the termination condition, the algorithm will output the individual with the smallest $F(x)$ and import it into CST for simulation verification. Table 1 shows the settings of important parameters in the optimization process. Each number in the target gain corresponds to the expected gain value of the frequency point in the optimization frequency band.

3 Experimental results

After selection, crossover and mutation by genetic algorithm, the final lens structure parameters are shown in Table 2. The coordinates of points 1, 7 and 8 are fixed (Figure 2B), and the coordinates of the other points are obtained by algorithm optimization. The distance between points 1 and 7 determines the thickness of the lens, and the distance between points 7 and 8 determines the aperture size of the lens. The lens has a diameter of 150 mm and a thickness of 30 mm at its thickest point. It is processed by 3D printing technology, and the actual structure is shown in Figure 3A. The lens is fed by a ridge horn antenna operating at 6–18 GHz. The horn antenna structure is shown in Figure 3B. The horn aperture size is 52 mm × 49 mm, and the distance from the lens aperture is 117 mm. Usually, the polarization mode of the horn antenna is linear polarization along the short side of the aperture surface, so the polarization mode of the feed antenna in this paper is linear polarization along the x-axis.

The phase center change of the horn antenna is shown in Figure 4A. It can be seen that the phase center has a certain change. The measured voltage standing-wave ratio (VSWR) of the horn

TABLE 3 Performance comparison of the proposed and existing antenna designs.

Reference	Aperture area (λ_0^2)	Aperture efficiency (%)	1-dB gain bandwidth (%)	Maximum gain (dBi)	Applied design method	Bandwidth (GHz)	Complexity	Applications
Liu et al. (2021)	12 × 12	11	29	23	Genetic algorithm	9–20	Moderate	UWB radar
Jeong and Ghalichechian (2020)	$\pi \times (6.9)^2$	10	6.7	22.5	Full-wave	29–31	High	RF identification, imaging systems
Lee and Lee (2023)	$\pi \times (3.38)^2$	55	7.4	23.9	ANSYS	12	High	FSS
Park and Lee (2021)	6.2 × 6.2	38	5.7	23	Optimized PCS and PEC sidewalls	5.8	High	MWPT
Yu et al. (2021)	$\pi \times (1.5)^2$	92.4	32.30	20.6	FDTD	13–18	Moderate	UWB radar
Ramazannia et al. (2018)	4.7 × 4.7	62	24.27	22.3	Full-wave	10.3	High	X-band
Proposed	$\pi \times (3)^2$	51.9	40	23.8	Genetic algorithm	6–18	Low	UWB

antenna and the lens antenna is shown in Figure 4B. It can be seen that the VSWR of the antenna after loading the lens deteriorates at some frequencies, which is mainly caused by the reflection of the lens. Figure 4C depicts the reflection coefficient (S_{11}) under different usage conditions. As can be seen from Figure 4C, the S_{11} when using the lens without horn has the best S_{11} whereas, the performance degrades when the horn is integrated with the lens but it is still in acceptable levels below −10 dB for most of the operating frequencies.

A 32-bit multitasking Windows® program, NSI2000 makes good use of the latest advancements in operating system technology to offer a wide range of capabilities (Wu and Ismail, 2024). A 3-D viewer is included with NSI2000 so that near-field and far-field data may be examined in a 3-D dynamic mode. The NSI2000 system was used to conduct actual measurements in a microwave darkroom, as shown in Figure 5. Only half of the directional pattern may be evaluated due to the test environment's constraints. Figure 6 displays the observed and simulated directional patterns of the feed and lens antennas. It can be seen that the simulated and measured directional patterns of the lens antenna are in good agreement, and the directivity of the antenna is significantly improved after the lens is loaded. In the simulation results, the beam widths of the antenna directional patterns after the lens is loaded are reduced by 38.1°/42.1°, 21.5°/33.4°, 23.2°/27.4°, and 21.2°/18.4° on the E and H planes at 6 GHz, 10 GHz, 14 GHz, and 18 GHz, respectively. There is a small error between the measured directional pattern and the simulated directional pattern. The main sources of error are: 1) The modeling error of the simulation model will introduce errors in the lens antenna, which can be eliminated by replacing the feed antenna; 2) There are certain deviations in the assembly and fixation of the horn antenna and the all-dielectric lens structure. In the actual measurement process, foam is used as a medium to fix the horn antenna and the lens (Zhou et al., 2024b). The thickness and dielectric constant of the medium will cause errors. The deformation of the foam during the fixation process will also cause errors; 3) The actual processing process has limited 3D printing accuracy, which will cause the rough surface of the dielectric lens to cause reflection of electromagnetic waves. PLA itself also has certain dielectric losses; 4) The NSI test system itself also has certain test errors.

The measured and simulated gain results of the horn antenna and lens antenna are shown in Figure 7. It can be seen that the simulated gain of the horn antenna in the 6–18 GHz frequency band is 8.3–15.5 dBi. After loading the dielectric lens (Yang et al., 2024), the gain of the lens antenna is 15.2–23.5 dBi, which is 10.7 dB higher than that of the horn antenna at 16 GHz. The measured gain of the lens antenna is 16.4–23.8 dBi, which is 6.4–10 dBi higher than that of the horn antenna. The 1-dB gain bandwidth is 12–18 GHz (relative bandwidth 40%). There are some differences between the simulation curve and the measured curve. The difference of the horn antenna mainly comes from the error of simulation modeling. The error sources of the lens antenna are mainly: the difference between the simulation and measurement of the feed antenna. Using the comparison method to test the gain, the error caused by the main lobe directions of the two antennas not being completely aligned when the transmitting and receiving antennas are fixed. Noise interference in the test environment. But overall, the gain trends of the simulation and measurement are consistent.

Aperture efficiency is an important indicator for judging the performance of aperture antennas, which can be obtained from Equation 2:

$$\eta_{ap} = \frac{G}{D_{max}}, D_{max} = \frac{4\pi A}{\lambda_0^2} \tag{2}$$

Where, G is the gain; D_{max} is the maximum directivity coefficient; A is the aperture area; λ_0 is the wavelength of free space. The simulation and measured results of the antenna aperture efficiency are shown in Figure 8. It can be seen that the simulated aperture efficiency of the lens antenna is greater than 28% in the working frequency band, and the simulated aperture efficiency reaches a maximum of 47.3% at 7 GHz. The measured results show that the aperture efficiency reaches 51.9% at 8 GHz, and the measured aperture efficiency is greater than 30% in the working frequency band. It can be seen that the measured aperture efficiency of the antenna is more seriously jittered. The main reasons for the jitter of the aperture efficiency curve are: the error of 3D printing lens processing, the lens and the antenna are fixed with foam, and the distance between the lens and the antenna has a certain error compared with the simulation.

Table 3 compares the performance of the antenna in this paper with high-gain antennas in recent relevant literature. It can be seen that this paper has widened the 1-dB gain bandwidth while ensuring high gain by setting the objective function. Compared with the literature (Liu et al., 2021; Jeong and Ghalichechian, 2020; Lee and Lee, 2023; Park and Lee, 2021), the proposed antenna has the smallest aperture area, the highest aperture efficiency, and the widest 1-dB gain bandwidth. Compared with the literature (Lee and Lee, 2023; Park and Lee, 2021; Yu et al., 2021; Ramazannia et al., 2018), although the proposed antenna has a larger aperture, but has a wider 1-dB gain bandwidth and a higher maximum gain.

4 Conclusion

This paper designs a broadband high-gain lens antenna based on genetic algorithm. First, an initial lens structure is designed, and optimized by genetic algorithm. A reasonable objective function is set to achieve high gain while widening the 1-dB gain bandwidth. The lens is processed by 3D printing technology, and the lens antenna is tested in a microwave darkroom. The test results show that the lens antenna works in the range of 6–18 GHz with a 1-dB gain bandwidth of 12–18 GHz (relative bandwidth 40%). The highest gain in the entire frequency band reaches 23.8 dBi at 18 GHz, which is 10 dBi higher than the feed horn antenna. The aperture efficiency of the entire frequency band is greater than 30%, and the maximum aperture efficiency is 51.9% at 8 GHz. Therefore, ultra-wideband, high gain, cheap cost, light weight, simple design and manufacture, and future ultra-wideband applications are some of the benefits of the proposed structure.

Data availability statement

The original contributions presented in the study are included in the article/supplementary material, further inquiries can be directed to the corresponding authors.

Author contributions

JZ: Conceptualization, Formal Analysis, Methodology, Resources, Software, Validation, Visualization, Writing–original draft, Writing–review and editing. SD: Conceptualization, Data curation, Formal Analysis, Investigation, Methodology, Resources, Validation, Writing–original draft, Writing–review and editing. DA: Conceptualization, Data curation, Investigation, Methodology, Project administration, Resources, Software, Supervision, Validation, Visualization, Writing–original draft, Writing–review and editing. IK: Conceptualization, Data curation, Formal Analysis, Investigation, Project administration, Resources, Supervision, Validation, Visualization, Writing–original draft, Writing–review and editing. P-CW: Conceptualization, Data curation, Formal Analysis, Resources, Software, Supervision, Validation, Visualization, Writing–original draft, Writing–review and editing. IH: Conceptualization, Data curation, Formal Analysis, Funding acquisition, Investigation, Project administration, Resources, Software, Supervision, Visualization, Writing–original draft, Writing–review and editing.

Funding

The author(s) declare that financial support was received for the research, authorship, and/or publication of this article. This work was supported by Princess Nourah bint Abdulrahman University Researchers Supporting Project number (PNURSP2024R435), Princess Nourah bint Abdulrahman University, Riyadh, Saudi Arabia. National Science and Technology Council 112-2811-E-005-011-MY2, 112-2634-F-005-001-MBK and 112-2634-F-005-002.

Conflict of interest

The authors declare that the research was conducted in the absence of any commercial or financial relationships that could be construed as a potential conflict of interest.

Publisher's note

References

Alibakhshikenari, M., Moghadasi, M., Sadeghzadeh, R., Virdee, B., and Limiti, E. (2016a). Traveling-wave antenna based on metamaterial transmission line structure for use in multiple wireless communication applications. *AEU-International J. Electron. Commun.* 70 (12), 1645–1650. doi:10.1016/j.aeue.2016.10.003

Alibakhshikenari, M., Moghadasi, M., Sadeghzadeh, R., Virdee, B., and Limiti, E. (2016b). Dual-band RFID tag antenna based on the Hilbert-curve fractal for HF and UHF applications. *IET Circuits, Devices and Syst.* 10 (2), 140–146. doi:10.1049/iet-cds.2015.0221

Alibakhshikenari, M., Moghadasi, M., Sadeghzadeh, R., Virdee, B., and Limiti, E. (2016c). A new planar broadband antenna based on meandered line loops for portable wireless communication devices. *Radio Sci.* 51 (7), 1109–1117. doi:10.1002/2016RS005973

Alibakhshikenari, M., Virdee, B., See, C., Alhameed, R., Falcone, F., and Limiti, E. (2019). Super-wide impedance bandwidth planar antenna for microwave and millimeter-wave applications. *Sensors* 19 (10), 2306–2309. doi:10.3390/s19102306

Alibakhshikenari, M., Virdee, B., Shukla, P., See, C., Alhameed, R., Falcone, F., et al. (2020). Improved adaptive impedance matching for RF front-end systems of wireless transceivers. *Sci. Rep.* 10 (14065), 1–11. doi:10.1038/s41598-020-71056-0

Alibakhshikenari, M., Virdee, B., Shukla, P., Wang, Y., Azpilicueta, L., Moghadasi, M., et al. (2021). Impedance bandwidth improvement of a planar antenna based on metamaterial-inspired T-matching network. *IEEE Access* 9, 67916–67927. doi:10.1109/ACCESS.2021.3076975

Beguad, X., Lepage, A., Varault, S., Soiron, M., and Barka, A. (2018). Ultra-wideband and wide-angle microwave metamaterial absorber. *Materials* 11 (10), 1–14. doi:10.3390/ma11102045

Chen, J., Wang, X., Fang, Z., Jiang, C., Gao, M., and Xu, Y. (2024). A real-time spoofing detection method using three low-cost antennas in satellite navigation. *Electronics* 13 (6), 1134. doi:10.3390/electronics13061134

Cicchetti, R., Cicchetti, V., Faraone, A., Foged, L., and Testa, O. (2020). A compact high-gain wideband lens Vivaldi antenna for wireless communications and through-the-wall imaging. *IEEE Trans. Antennas Propag.* 69 (6), 3177–3192. doi:10.1109/TAP.2020.3037777

Dai, M., Luo, L., Ren, J., Yu, H., and Sun, G. (2022). PSACCF: prioritized online slice admission control considering fairness in 5G/B5G networks. *IEEE Trans. Netw. Sci. Eng.* 9 (6), 4101–4114. doi:10.1109/TNSE.2022.3195862

Dai, M., Sun, G., Yu, H., and Niyato, D. (2024). Maximize the long-term average revenue of network slice provider via admission control among heterogeneous slices. *IEEE/ACM Trans. Netw.* 32 (1), 745–760. doi:10.1109/TNET.2023.3297883

Fan, Y., Wang, J., Li, Y., Zhang, J., Qu, S., Han, Y., et al. (2018). Frequency scanning radiation by decoupling spoof surface plasmonpolaritons via phase gradient metasurface. *IEEE Trans. Antennas and Propag.* 66 (1), 203–208. doi:10.1109/tap.2017.2767625

Farooq, U., Iftikhar, A., Shafique, M., Khan, M., Fida, A., Mughal, M. J., et al. (2021). C-band and X-band switchable frequency-selective surface. *Electronics* 10 (4), 1–15. doi:10.3390/electronics10040476

Feng, P., Qu, S., and Yang, S. (2019). Defocused cylindrical Luneburg lens antennas with phased array antenna feed. *IEEE Trans. Antennas Propag.* 67 (9), 6008–6016. doi:10.1109/tap.2019.2920319

Ge, S., Zhang, Q., Chiu, C., Chen, Y., and Murch, R. D. (2018). Single side scanning surface waveguide leaky-wave antenna using spoof surface plasmon excitation. *IEEE Access* 6, 66020–66029. doi:10.1109/access.2018.2879086

Hao, J., Yang, X., Wang, C., Tu, R., and Zhang, T. (2022). An improved NSGA-II algorithm based on adaptive weighting and searching strategy. *Appl. Sci.* 12 (22), 1–16. doi:10.3390/app122211573

Hao, Z., Zhang, J., and Zhao, L. (2019). A compact leaky-wave using a planar spoof surface plasmonpolariton structure. *Int. J. RF Microw. Computer-Aided Eng.* 29 (5), 1–7. doi:10.1002/mmce.21617

Ikram, M., Sultan, K., Mobashsher, A., Moosazadeh, M., and Abbosh, A. (2024). Wide-angle beam steering closed-form pillbox antenna fed by substrate-integrated waveguide horn for on-the-move satellite communications. *Sensors* 24 (3), 1–14. doi:10.3390/s24030732

Jeong, K., and Ghalichechian, N. (2020). 3D-printed 4-zone Ka-band Fresnel lens: design, fabrication, and measurement. *IET Microwaves, Antennas Propag.* 14 (1), 28–35. doi:10.1049/iet-map.2019.0117

Karami, F., Boutayeb, H., Elahi, A., Ghayekhloo, A., and Talbi, L. (2022). Developing broadband microstripe patch antennas fed by SIW feeding network for spatially low cross-polarization. *Sensors* 22 (9), 1–14. doi:10.3390/s22093268

Khan, S., Malik, A., Velioglu, B., Gul, S., Kavakli, I., and Lazoglu, I. (2024). A novel smart disinfection system using 3D-printed and electrically conductive composite hydrogel. *Emergent Mater.* 8 (1), 1–16. doi:10.1007/s42247-024-00632-1

Kumar, C., Raghuwanshi, S., and Kumar, V. (2022). Graphene based microstrip patch antenna on photonic crystal substrate for 5G application. *Front. Mater.* 9, 1–11. doi:10.3389/fmats.2022.1079588

Kumar, N., Naidu, K., Banerjee, P., Babu, T., and Reddy, B. (2021). A review on metamaterials for device applications. *Crystals* 11 (5), 1–16. doi:10.3390/cryst11050518

Lee, G., Kumar, S., Choi, H., and Kim, K. W. (2021). Wideband high-gain double-sided dielectric lens integrated with a dual-bowtie antenna. *IEEE Antennas Wirel. Propag. Lett.* 20 (3), 293–297. doi:10.1109/lawp.2020.3048165

Lee, J., and Lee, H. (2023). Low-profile high-efficiency transmitarray antenna for beamforming applications. *Electronics* 12 (14), 1–10. doi:10.3390/electronics12143178

Lee, W., and Yoon, Y. (2017). A broadband dual-metallic-reflect array antenna for millimeter-wave applications. *IEEE Antennas Wirel. Propag. Lett.* 16, 856–859. doi:10.1109/LAWP.2016.2610002

Li, M., Wang, T., Chu, F., Han, Q., Qin, Z., and Zuo, M. J. (2021). Scaling-basis chirplet transform. *IEEE Trans. Industrial Electron.* 68 (9), 8777–8788. doi:10.1109/TIE.2020.3013537

Li, X., Wang, G., Zou, X., Li, T., and Cai, T. (2023). Broadband circularly polarized folded transmitarray antenna based on polarization conversion metasurfaces. *AEU-International J. Electron. Commun.* 163, 154596–154615. doi:10.1016/j.aeue.2023.154596

Li, Y., Luo, Y., Wu, X., Shi, Z., Ma, S., and Yang, G. (2024). Variational bayesian learning based localization and channel reconstruction in RIS-aided systems. *IEEE Trans. Wirel. Commun.* 23, 11309–11324. doi:10.1109/TWC.2024.3380903

Liu, F., Zhao, X., Zhu, Z., Zhai, Z., and Liu, Y. (2023). Dual-microphone active noise cancellation paved with Doppler assimilation for TADS. *Mech. Syst. Signal Process.* 184, 109727. doi:10.1016/j.ymssp.2022.109727

Liu, L., Wang, J., Yin, X., and Chen, Z. (2018). Wide-angle beam scanning leaky-wave antenna using spoof surface plasmonpolaritons structure. *Electronics* 7 (12), 1–11. doi:10.3390/electronics7120348

Liu, X., Peng, L., Liu, Y., Yu, W., Zhao, Q., Jiang, X., et al. (2021). Ultra-broadband all dielectric transmitarray designing based on genetic algorithm optimization and 3D print technology. *IEEE Trans. Antennas Propag.* 69 (4), 2003–2012. doi:10.1109/TAP.2020.3026922

Park, J., and Lee, J. (2021). Low-profile high efficiency transmitarray antenna using optimized phase compensation surface (PCS) and PEC sidewalls. *ICT Express* 7 (4), 501–506. doi:10.1016/j.icte.2021.04.002

Poyanco, J., Pizarro, F., and Iglesias, E. (2022). Cost-effective wideband dielectric planar lens antenna for millimeter wave applications. *Sci. Rep.* 12 (4204), 1–15. doi:10.1038/s41598-022-07911-z

Rahman, A., Kamardin, K., Yamada, Y., and Takahashi, M. (2024). Design method of a focusing dielectric lens antenna and temperature increment measurement at the focusing spot. *Heliyon* 10 (6), 1–13. doi:10.1016/j.heliyon.2024.e28061

Ramazannia, T., Rezaei, P., and Tavakkol, H. (2018). High-efficient wideband transmitarray antenna. *IEEE Antenna Wirel. Propag. Lett.* 17 (5), 817–820. doi:10.1109/LAWP.2018.2817363

Sadeghzadeh, R., Alibakhshikenari, M., and Moghadasi, M. (2016). UWB antenna based on SCRLH-TLs for portable wireless devices. *Microw. Opt. Technol. Lett.* 58 (1), 69–71. doi:10.1002/mop.29491

Soliman, S., Eldesouki, E., and Attiya, A. (2022). Analysis and design of an X-band reflectarray antenna for remote sensing satellite system. *Sensors* 22 (3), 1–18. doi:10.3390/s22031166

Srivastava, H., Singh, A., Rajeev, A., and Tiwari, U. (2020). Bandwidth and gain enhancement of rectangular microstrip patch antenna (RMPA) using slotted array technique. *Wirel. Personal. Commun.* 114 (3), 699–709. doi:10.1007/s11277-020-07388-x

Sun, G., Sheng, L., Luo, L., and Yu, H. (2022). Game theoretic approach for multipriority data transmission in 5G vehicular networks. *IEEE Trans. Intelligent Transp. Syst.* 23 (12), 24672–24685. doi:10.1109/TITS.2022.3198046

Sun, G., Xu, Z., Yu, H., and Chang, V. (2021). Dynamic network function provisioning to enable network in box for industrial applications. *IEEE Trans. Industrial Inf.* 17 (10), 7155–7164. doi:10.1109/TII.2020.3042872

Ullah, S., Ruan, C., Haq, T., and Zhang, X. (2019). High performance THz patch antenna using photonic band gap and defected ground structure. *J. Electromagn. Waves Appl.* 33 (15), 1943–1954. doi:10.1080/09205071.2019.1654929

Wang, C., Wen, P., Huang, X., Chen, K., and Xu, K. (2024d). Terahertz dual-band bandpass filter based on spoof surface plasmon polaritons with wide upper stopband suppression. *Opt. Express* 32 (13), 22748–22758. doi:10.1364/OE.525298

Wang, J., Duan, J., Shen, X., Wang, Y., and Zhang, B. (2024a). Miniaturized lens antenna with enhanced gain and dual-focusing for millimeter-wave radar system. *Micromachines* 15 (3), 1–10. doi:10.3390/mi15030335

Wang, M., Wang, B., Zhang, R., Wu, Z., and Xiao, X. (2023). Flexible Vis/NIR wireless sensing system for banana monitoring. *Food Qual. Saf.* 7. doi:10.1093/fqsafe/fyad025

Wang, Q., Sihvola, A., and Qi, J. (2024b). A novel procedure to hybridize the folded transmitarray and fabry–perot cavity with low antenna profile and flexible design frequency. *IEEE Antennas Wirel. Propag. Lett.* 23 (8), 2501–2505. doi:10.1109/LAWP.2024.3398076

Wang, Y., Xiao, R., Xiao, N., Wang, Z., Chen, L., Wen, Y., et al. (2022). Wireless multiferroic memristor with coupled giant impedance and artificial synapse application. *Adv. Electron. Mater.* 8 (10), 2200370. doi:10.1002/aelm.202200370

Wang, Y., Yu, A., Cheng, Y., and Qi, J. (2024c). Matrix diffractive deep neural networks merging polarization into meta-devices. *Laser and Photonics Rev.* 18 (2), 2300903. doi:10.1002/lpor.202300903

Wen, C., Huang, Y., Peng, J., Wu, J., Zheng, G., and Zhang, Y. (2022). Slow-time FDA-MIMO technique with application to STAP radar. *IEEE Trans. Aerosp. Electron. Syst.* 58 (1), 74–95. doi:10.1109/TAES.2021.3098100

Wen, P., Jiang, Y., Liu, F., Ma, Z., and Wang, Y. (2024b). Direct synthesis of continuously tunable wideband bandpass filtering attenuator with multiple transmission zeros. *IEEE Trans. Circuits Syst. II Express Briefs* 71, 4346–4350. doi:10.1109/TCSII.2024.3386034

Wen, P., Jiang, Y., Liu, F., Wang, C., Ma, Z., and Wang, Y. (2024a). Synthesis design of high-selectivity wideband balanced bandpass filter based on parallel coupled lines. *AEU - Int. J. Electron. Commun.* 176, 155159. doi:10.1016/j.aeue.2024.155159

Wu, Z., and Ismail, M. (2024). Generalized RIS tile exclusion strategy for indoor mmWave channels under concept drift. *IEEE Trans. Wirel. Commun.*, 1. doi:10.1109/TWC.2024.3402267

Xiao, N., Wang, Y., Chen, L., Wang, G., Wen, Y., and Li, P. (2023). Low-frequency dual-driven magnetoelectric antennas with enhanced transmission efficiency and broad bandwidth. *IEEE Antennas Wirel. Propag. Lett.* 22 (1), 34–38. doi:10.1109/LAWP.2022.3201070

Xiao, X., He, Q., Li, Z., Antoce, A. O., and Zhang, X. (2017). Improving traceability and transparency of table grapes cold chain logistics by integrating WSN and correlation analysis. *Food control.* 73 (Part B), 1556–1563. doi:10.1016/j.foodcont.2016.11.019

Yang, H., Chen, D., Mao, Y., and Yang, J. (2020). Tunable broadband THz waveband absorbers based on graphene for digital coding. *Nanomaterials* 10 (9), 1–12. doi:10.3390/nano10091844

Yang, M., Cai, C., Wang, D., Wu, Q., Liu, Z., and Wang, Y. (2024). Symmetric differential demodulation-based heterodyne laser interferometry used for wide frequency-band vibration calibration. *IEEE Trans. Industrial Electron.* 71 (7), 8129–8137. doi:10.1109/TIE.2023.3299015

Yang, Y., Wei, X., Yao, W., and Lan, J. (2023b). Broadband electrical impedance matching of sandwiched piezoelectric ultrasonic transducers for structural health monitoring of the rail in-service. *Sensors Actuators A Phys.* 364, 114819. doi:10.1016/j.sna.2023.114819

Yang, Y., Zhang, Z., Zhou, Y., Wang, C., and Zhu, H. (2023a). Design of a simultaneous information and power transfer system based on a modulating feature of magnetron. *IEEE Trans. Microw. Theory Tech.* 71 (2), 907–915. doi:10.1109/TMTT.2022.3205612

Yu, W., Peng, L., Liu, Y., Zhao, Q. x., Jiang, X., and Li, S. m. (2021). An ultra-wideband and high aperture efficiency all-dielectric lens antenna. *IEEE Antennas Wirel. Propag. Lett.* 20 (12), 2442–2446. doi:10.1109/LAWP.2021.3114159

Zha, S., Qu, Z., Zhang, J., Zheng, D., and Liu, P. (2024). A gain reconfigurable reflector antenna with surface mounted field-induced artificial magnetic conductor for adaptive HIRF prevention. *IEEE Trans. Antennas Propag.* 72, 7252–7260. doi:10.1109/TAP.2024.3434371

Zhang, Y., Zhao, P., Lu, Q., Zhang, Y., Lei, H., Yu, C., et al. (2023). Functional additive manufacturing of large-size metastructure with efficient electromagnetic absorption and mechanical adaptation. *Compos. Part A Appl. Sci. Manuf.* 173, 107652. doi:10.1016/j.compositesa.2023.107652

Zhou, D., Sheng, M., Bao, C., Hao, Q., Ji, S., and Li, J. (2024b). 6G non-terrestrial networks-enhanced IoT service coverage: injecting new vitality into ecological surveillance. *IEEE Netw.* 38 (4), 63–71. doi:10.1109/MNET.2024.3382246

Zhou, Y., Xie, J., Zhang, X., Wu, W., and Kwong, S. (2024a). Energy-efficient and interpretable multisensor human activity recognition via deep fused lasso net. *IEEE Trans. Emerg. Top. Comput. Intell.*, 1–13. doi:10.1109/TETCI.2024.3430008